Results in Engineering 20 (2023) 101473

Contents lists available at ScienceDirect

Results in Engineering

journal homepage: www.sciencedirect.com/journal/results-in-engineering

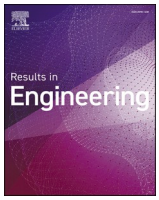

Mini-channel cooling system for solar PV Panels with hybrid magnetic nanofluid and magnetic field

Suvanjan Bhattacharyya [a], Naman Jain [a], Tapasvi Bhatt [a], Humaira Yasmin [b], Mohsen Sharifpur [c,d,*]

[a] Department of Mechanical Engineering, Birla Institute of Technology and Science Pilani, Pilani Campus, Vidya Vihar, Pilani, 333 031, Rajasthan, India
[b] Department of Basic Sciences, Preparatory Year Deanship, King Faisal University, Al-Ahsa, 31982, Saudi Arabia
[c] Department of Mechanical and Aeronautical Engineering, University of Pretoria, Pretoria, 0002, South Africa
[d] Department of Medical Research, China Medical University Hospital, China Medical University, Taichung, Taiwan

ARTICLE INFO

Keywords:
Non-uniform magnetic field
Heat transfer enhancement
Hybrid nanofluid
Mini-channel. PV panel cooling

ABSTRACT

This study delves into the interplay between magnetic fields, heat transfer, and fluid behavior within a 3D mini-channel. Exploring the effects of a magnetic field on a hybrid nanofluid (Fe_3O_4–TiO_2) under varying intensities (1000–2000 Gauss) and positions. Using numerical simulations (finite volume method), key parameters like Nusselt number (*Nu*), Friction factor (f), and Thermal Enhancement Factor (TEF) have been analyzed to uncover how magnetic fields and nanofluids interact in complex geometries. Results showed that the application of a magnetic field significantly enhanced heat transfer performance, with a maximum Nusselt number enhancement of 230%. Moreover, it was shown that greater magnetic field intensities were associated with elevated friction factors, whereas friction factors exhibited a declining trend as Reynolds numbers increased. The thermal enhancement factor initially increased with Reynolds numbers, but declined after reaching a peak. However, higher magnetic field strengths mitigated this decline, intensifying heat transfer enhancement effects reaching a maximum of 2.18 at 2000G magnetic field. These findings provide quantitative insights into the effectiveness of magnetic fields in enhancing heat transfer in Fe_3O_4–TiO_2 hybrid nanofluids.

1. Introduction

The world is currently grappling with an energy crisis that affects nations across the globe. As

Populations grow and industrialization expands, the energy demand continues to escalate while traditional fossil fuel reserves dwindle. This pressing global issue necessitates exploring innovative and sustainable approaches to meet the ever-increasing energy requirements of our society. In this context, optimizing heat transfer (HT) processes becomes paramount, as it directly impacts the efficiency and performance of various energy systems.

Efficient heat transfer plays a crucial role in a wide range of applications, including power generation [1], electronics cooling [2], thermal management in aerospace [3], and chemical processes [4]. Improving heat transfer can enhance energy efficiency, reduce operational costs, and minimise environmental footprint. Therefore, It is imperative to develop strategies that optimize heat transfer to meet the growing energy demands while striving for a more sustainable future. Heat transfer mechanisms may be broadly categorized into active and passive methods. Passive techniques, such as natural convection, radiation, and conduction, rely on the physical properties and inherent characteristics of the materials involved. Passive devices have been used for a long time due to their low cost, as they do not require any external energy sources, simple disassembly, and maintenance. Among these devices, twisted tapes [5,6] stand as a compelling strategy to enhance fluid mixing and convective heat transfer. Similarly, incorporating coiling wires [7] introduces intricate flow patterns that augment heat exchange efficiency. Fins [8] emerge as a classic choice, effectively amplifying heat transfer surface area to optimize convective processes. Applying dimples [9] on surfaces triggers-controlled turbulence, further intensifying heat transfer mechanisms.

Rib structures [10] find relevance in both compact heat exchangers and channel flow configurations, promoting turbulence and enhancing convective heat transfer. Baffles [11], strategically positioned, create disruption in flow, encouraging mixing and heat exchange enhancement. Vortex generators [12–14] play a pivotal role in inducing swirl

* Corresponding author. Department of Mechanical and Aeronautical Engineering, University of Pretoria, Pretoria, 0002, South Africa.
E-mail addresses: suvanjan.bhattacharyya@pilani.bits-pilani.ac.in (S. Bhattacharyya), mohsen.sharifpur@up.ac.za (M. Sharifpur).

https://doi.org/10.1016/j.rineng.2023.101473
Received 10 August 2023; Received in revised form 27 September 2023; Accepted 28 September 2023
Available online 29 September 2023

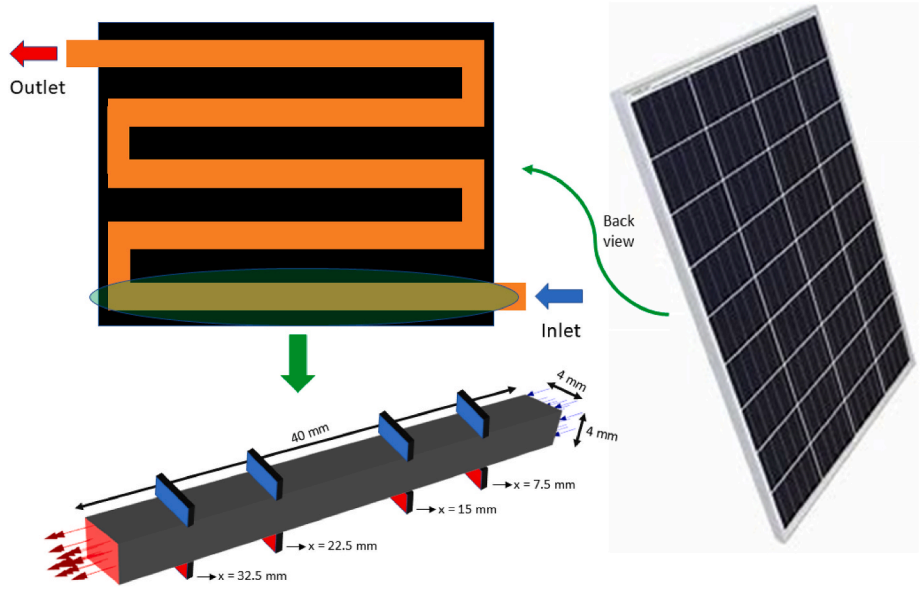

Fig. 1. Schematic diagram.

and vortices, accelerating convective heat transfer rates in various fluid systems. Wings [15] and winglets [16], often utilized in airfoil design, introduce controlled aerodynamic interactions that bolster heat transfer performance.

In tandem with these innovative designs, the realm of passive heat transfer enhancement has been invigorated by the advent of nanofluids [17–20]. Nanofluids exhibit remarkable thermal conductivity and convective heat transfer augmentation by leveraging the dispersal of nanoparticles within a base fluid. These materials present an exciting avenue for bolstering heat exchange in a wide array of applications. Nanofluids, which are colloidal suspensions of nanoparticles (NPs) in a base fluid, offer unique advantages due to the nanoparticles' enhanced thermal conductivity and convective heat transfer properties. When nanoparticles are distributed in the water, they significantly increase the effective thermal conductivity, allowing for more efficient heat dissipation.

While passive methods are effective in certain scenarios [21–23], they often have limitations when it comes to achieving high heat transfer rates or enhancing the performance of specific systems. To overcome these limitations, active techniques that actively manipulate heat transfer processes have gained significant attention. Active techniques involve the application of external forces or fields to augment heat transfer. These methods offer the potential to overcome the limitations of passive methods by actively manipulating the heat transfer processes and optimizing energy transfer. Forced convection, for instance, utilizes external fans or pumps to increase the fluid flow rate and enhance heat transfer rates. Electrohydrodynamics is another active technique that uses electric fields to induce fluid motion, improving heat transfer. The applied voltage is more efficient for natural convection flow at reduced heat fluxes and low Reynolds numbers. Acoustic methods utilize sound waves to enhance heat transfer by creating fluid agitation and enhancing mixing [24,25].

One particularly promising avenue for heat transfer enhancement is using magnetic

fields. Magnetic fields have been found to significantly influence heat transfer characteristics. They can induce fluid motion, alter the behavior of heat transfer fluids, and enhance convective heat transfer rates. By employing non-uniform magnetic fields, researchers have achieved remarkable improvements in heat transfer performance, offering new possibilities for efficient energy utilization.

Bezaatpour and Goharkhah [26] proposed a method using an external magnetic field to enhance HT in heat exchangers (HEX) by generating a swirling flow in the magnetic working fluid. Their numerical simulation showed a HT enhancement of up to 320% with minimal pressure drop increase. Bezaatpour and Rostamzadeh [27] investigated the influence of an external magnetic field with Fe_3O_4/-water nanofluid on a fin-and-tube compact HEX. They found a HT enhancement of 8.7%–52.4% with a subtle pressure drop increment. Lei et al. [28] analyzed the potential of magnetohydrodynamic (MHD) convection to increase HT during magnetic cooling. They achieved a HT enhancement of about 40% by creating a swirling flow with an external magnetic field.

Sharma et al. [29,30] conducted two studies on the impact of magnetic fields on thermal and flow performance. The first study found heat transfer enhancements of 6.13%–37.38% with varying magnetic field strengths, accompanied by increased pressure drop (PD) due to vortex formation.

In the second study, magnetic fields increased the Nusselt number by 4.95%–19.27%, but also increased the PD. The TEF increased by 9.53%–12.50%, and TEF values were generally greater than unity for a wide range of inclinations with magnetic fields.

Sheikholeslami et al. [31] conducted experimental research on nano-refrigerant boiling heat transfer and observed increased heat transfer coefficient with increasing flattened percentage and nanoparticle concentration. Kumar et al. [32] developed a numerical model considering a magnetic field, thermal radiation, and viscous dissipation. They found that increasing the radiation parameter improved velocity and temperature profiles. Pordanjani et al. [33] evaluated the influence of radiation on convective HT and entropy formation in a diagonal rectangular container that included a magnetic field. They observed that HT and entropy generation increased with the Rayleigh number (Ra) and decreased with the magnetic field angle.

The current investigation presents several novel aspects in the investigation of HT characteristics in a three-dimensional mini-channel with a square cross-section when subjected to the influence of a magnetic field. To begin, in contrast to earlier studies, which concentrated their attention primarily on two-dimensional (2D) or simplified geometries, the current study specifically investigates the intricate three-dimensional nature of the mini-channel. The study provides a more comprehensive understanding of the behaviour of heat transfer in complex flow configurations, which better represents applications that occur in the real world, as a result of taking into account the full three-dimensional aspect.

Second, this research investigates how the performance of HT can be

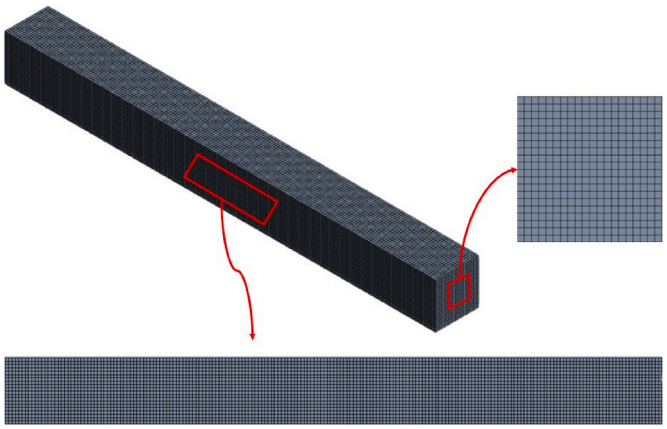

Fig. 2. Domain discretization.

affected by changing the magnetic field strength as well as the position of the magnets at different Reynolds number of 75, 85, 95, 105, 125, 150, 170 and 190. An in-depth study of the effect that these parameters have on the HT characteristics is carried out by systematically altering the magnetic field strength from 1000G to 2000G and adjusting the magnet position within the 40 mm channel length. This allows for the study to provide accurate results. The utilization of a hybrid nanofluid that is made up of 1% Fe_3O_4 nanoparticles and 1% TiO_2 nanoparticles is another aspect of the present work that contributes to its novel nature. The addition of nanoparticles to the working fluid results in the introduction of additional complexities, such as nanoparticle aggregation and interparticle interactions, both of which have the potential to have a significant impact on the manner in which heat is transferred.

2. Computational methodology

This study employs four magnets placed at different positions along the mini-channel. The heat transfer properties of the channel were determined by analysing a set of scenarios. The system is defined by a set of source configurations that include: (i) a single source positioned at 7.5 mm; (ii) a single source positioned at x = 15 mm; (iii) a single source positioned at x = 25 mm; (iv) two sources positioned at x = 25 mm and 32.5 mm; and (v) four sources positioned at x = 7.5 mm, 15 mm, 25 mm, and 32.5 mm, as depicted in the Fig. 1.

The rationale behind favoring symmetric magnet placement is rooted in its capacity to ensure uniform heat distribution along the length of the channel. By strategically positioning magnets in a symmetrical manner a balanced distribution of heat transfer enhancement effects is achieved, thereby avoiding localized or uneven heating. This, in turn, contributes to a more controlled and predictable heat transfer process, which is crucial for maintaining accurate experimental results.

Moreover, the adoption of symmetric magnet placement has the added benefit of reducing the likelihood of flow disturbances or turbulent behaviors caused by uneven magnetic field distribution. These disturbances can impede the desired heat transfer enhancement effects and introduce complexities into the experimental setup.

Various Reynolds numbers (Re) and magnetic field strengths are utilized to test each configuration. Each magnet functions as a theoretical obstruction whose vertical dimension is contingent upon the intensity of the magnetic force. The augmentation of magnet quantity results in increased turbulence, thereby leading to an increase in HT. However, as a result of the formation of eddies, there is also an increase in pressure drop.

2.1. Geometry and grid generation

The 3D mini-channel depicted in the figure has a square cross-section

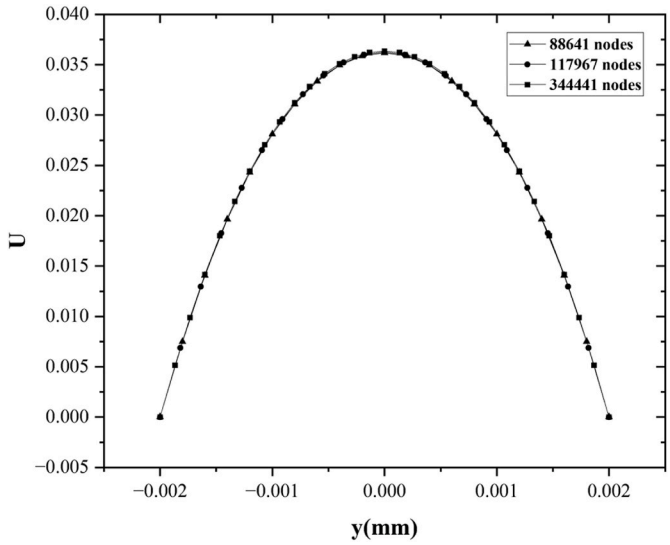

Fig. 3. Grid independence test.

of 4 mm and a length of 40 mm. All surfaces, except for the bottom surface, exhibit adiabatic behaviour, while the bottom surface maintains isothermal conditions. The Fe_3O_4–TiO_2 nanofluid functions as a homogeneous coolant with consistent inlet velocity and temperature, flowing evenly through the channel. A computational grid consisting of 88641 cube shaped nodes was chosen to accurately measure the velocity and thermal gradient within the flow domain (see Fig. 2). Grid independence test was performed with multiple grid sizes using ratio of velocity at center of the channel to the inlet velocity as shown in Fig. 3. Among the various potential grid configurations considered, the 88641 cube shaped nodes grid configuration was chosen as the preferred option. The decision was made with the dual objective of reducing processing time and achieving reliable outcomes.

2.2. Boundary conditions

The top surface of the mini-channel is entirely insulated while keeping the bottom surface isothermally maintained at 350K. All the other surfaces were treated as adiabatic walls. At the channel boundaries, no-slip velocity and temperature jump conditions were designated. In all cases, the channel inlet was maintained at a constant temperature of 293K. The outflow of the channel maintained a constant atmospheric pressure throughout the simulations.

It is essential to treat nanofluid properties as a function of temperature and nanoparticle concentration. The hybrid nanofluid comprises of 1% Fe_3O_4 and 1% TiO_2 with water as the base fluid. Under the assumption that the nanoparticle concentration is uniform across the domain, the effective physical properties of nanofluid can be calculated as follows [34]:

$$\rho_{nf} = (1-\varphi)\rho_f + \varphi\rho_{np} \tag{1}$$

$$\left(\rho C_p\right)_{nf} = (1-\varphi)\left(\rho C_p\right)_f + \varphi\left(\rho C_p\right)_{np} \tag{2}$$

$$\mu_{nf} = \mu_f(1+2.5\varphi) \tag{3}$$

$$k_{nf} = k_{static} + k_{brownian} \tag{4}$$

where,

$$k_{static} = k_f\left[\frac{\left(k_{np}+2k_f\right)-2\varphi\left(k_f-k_{np}\right)}{\left(k_{np}+2k_f\right)+\varphi\left(k_f-k_{np}\right)}\right] \tag{5}$$

$$k_{brownian} = 5 * 10^4 \beta\varphi\rho_f C_{p,f}\sqrt{\frac{kT}{\rho_{nf}D_{np}}}g(\varphi,T) \quad (6)$$

where k indicates Boltzmann constant, φ represents nanoparticle concentration, β depicts the liquid volume fraction and g denotes the modelling function given by Ref. [35]:

$$g(\varphi,T) = (-6.04\varphi + 0.4705)T + 1722.3\varphi - 134.63 \quad (7)$$

For greater precision, the physical properties of the base fluid, water in the present analysis, are assumed to be a function of temperature. They are provided by Ref. [35]:

$$\rho_f = 2446 - 20.674T + 0.11576T^2 - 3.12895 \times 10^{-4}T^3 + 4.0505 \times 10^{-7}T^4 - 2.0546 \times 10^{-10}T^5 \quad (8)$$

$$\mu_f = 2.414 \times 10^{-5} \times 10^{\left[\frac{247}{T-140}\right]} \quad (9)$$

$$k_f = -1.13 + 9.71 \times 10^{-3}T - 1.31 \times 10^{-5}T^2 \quad (10)$$

2.3. Mathematical and computational implementations

The present study employs a computational implementation model that specifically targets the section of the fluid domain ranging from the intake to a location situated 40 mm downstream. The model utilized in this study also made substantial efforts to achieve a considerable level of solution accuracy, particularly in close proximity to the fluid domain. The aforementioned outcome was attained through existing literature and exhaustive method of discretization, as indicated by the successful satisfaction of convergence conditions. The convergence criteria for the variables x-velocity, y-velocity, z-velocity, and continuity were set at a threshold of 10^{-5}, whereas a greater level of precision, 10^{-6}, was sought for energy convergence.

2.4. Numerical modelling

The present study employs ANSYS FLUENT 18.1 commercial software to carry out numerical simulations. In this study, the laminar viscous model has been employed in conjunction with the COUPLED method for pressure-velocity coupling. The stability of the main flow was evaluated. The finite-volume method is used to discretize the governing equations of fluid flow and HT, and the resulting algebraic equations are solved using an iterative algorithm. In this study, the discretization of the momentum equations was carried out using a second-order upwind scheme. Additionally, the energy equation was discretized using the QUICK scheme, as per which structured meshes are aligned with the flow direction, yielding higher accuracy when utilized.

By utilizing this scheme, we aim to improve the accuracy and efficiency of our numerical simu-lations. The described CFD solver simulates fluid flow and HT in engineering applications reliably and efficiently. This study aims to investigate the phenomenon of flow at extremely low Reynolds numbers. Specifically, the Reynolds numbers considered in this study are 75, 85, 95, 105, 125, 150, 170, and 190, which are calculated based on the channel width.

The assumptions underlying the numerical model for fluid flow and heat transfer in the square channel includes, steady flow, laminar flow, fully developed flow, incompressible flow, neglect of body forces, neglect of thermal radiation and neglect of viscous dissipation.

These assumptions form the basis for the simplified mathematical representation of fluid flow and heat transfer in the square channel, making it possible to derive the governing equations for further analysis and numerical simulations as follows [36]:

Table 1
Nomenclature.

Symbol	Description
B	Magnetic Field Strength (Gauss)
C_p	Specific Heat Transfer Coefficient (J/kg/K)
D	Hydraulic diameter (m)
F	Friction factor
G	Modelling Function
h	Heat transfer coefficient (W/m^2 K)
j	Colburn j- factor
k	Thermal Conductivity (Wm^{-1} K^{-1})
L	Length of Mini-channel (mm)
Nu	Nusselt number
Δp	Pressure difference
Pr	Prandtl Number
Re	Reynolds number
T	Temperature (K)
TEF	Thermal enhancement factor
u	Horizontal velocity (m/s)
u_i	Velocity in x_i direction
u_j	Velocity in x_j direction
x, y, z	Directions
Greek symbols:	
P	Density (kgm^{-3})
μ	Dynamic Viscosity (Pas)
φ	Nanoparticle Concentration
φ'	Average value at the top and bottom boundaries
φ_x'	Local value of φ' at a distance x from the inlet
ν	Kinematic Viscosity (m^2 s^{-1})
β	liquid volume fraction (k^{-1})
Γ	Thermal Diffusivity (m^{2}s^{-1})
Subscripts:	
o	Reference condition (without magnetic field)
f	Fluid
m	In presence of Magnetic Field
np	Nanoparticle
nf	Nanofluid
x	Distance from inlet

Table 2
Properties of Fe_3O_4 and TiO_2 nanoparticles [8,20].

Property	Fe_3O_4	TiO_2
ρ	4950 kg/m^3	4175 kg/m^3
C_p	640 J/kgK	692 J/kgK
k	7 W/m.K	8.4 W/m.K

$$\text{Continuity Equation [36]}: \frac{\partial}{\partial x_i}(\rho u_i) = 0 \quad (11)$$

$$\text{Momentum Equation [36]}: \frac{\partial(\rho u_i u_j)}{\partial x_j} = -\frac{\partial p}{\partial x_i} + \frac{\partial}{\partial x_j}\left[\mu\frac{\partial u_i}{\partial x_j} + \mu\frac{\partial u_j}{\partial x_i}\right] \quad (12)$$

$$\text{Energy Equation [36]}: \frac{\partial(\rho u_i T)}{\partial x_i} = \frac{\partial}{\partial x_j}\left[\Gamma\frac{\partial T}{\partial x_j}\right] \quad (13)$$

Here, Γ represents the thermal diffusivity [36]:

$$\Gamma = \frac{\mu}{Pr} \quad (14)$$

3. Data reduction and validation

In this section, various equations and correlations were presented to analyze and validate the data (see Table 1). The properties of nanoparticles used in the present study have been summarized in Table 2. The *Nu* and *f* were defined as follows:

The *Nu*, which represents the ratio of convective to conductive HT, was given by:

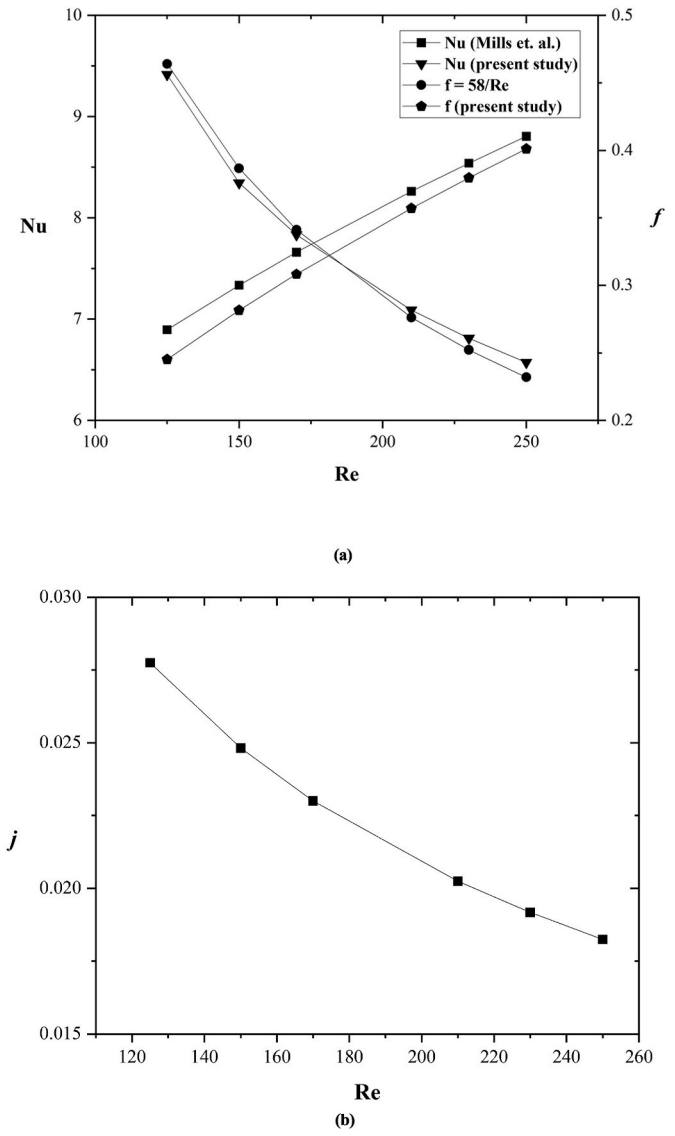

Fig. 4. (a) Validation of the model used in present study with established correlations by Mills [37] and Experimental setup [39], and (b) Colburn j-factor for the plain channel is the function of Reynolds number.

$$Nu = \frac{hD}{k} \tag{15}$$

The f was determined based on the PD in the channel and was expressed as:

$$f = \frac{\Delta P}{\frac{1}{2}\rho u^2 \frac{L}{D}} \tag{16}$$

The Nusselt number correlation proposed by Mills [37] was given by:

$$Nu = 3.66 + \frac{0.065 RePr\frac{D}{L}}{1 + 0.04\left[RePr\frac{D}{L}\right]^{\frac{2}{3}}} \tag{17}$$

The Colburn j-factor characterizing the convective heat transfer in a fluid is given by Ref. [38]:

$$j = \frac{Nu}{RePr^{\frac{1}{3}}} \tag{18}$$

The equation for laminar flow was given by Ref. [39]:

$$f = \frac{58}{Re} \tag{19}$$

Furthermore, the thermal performance factor (TEF) was evaluated using the following equation:

$$TEF = \frac{\frac{Nu}{Nu_o}}{\left(\frac{f}{f_o}\right)^{\frac{1}{3}}} \tag{20}$$

These equations and correlations served to reduce and validate the data, providing a reliable basis for further analysis in the present study. The Nusselt number obtained from the Fluent model deployed for this study was compared with the Nusselt number correlation by Mills [37]. Additionally, the friction factor obtained from the PD across the length of the channel was compared with the correlation given by experimental result and analysis [39]. The comparison results are presented in Fig. 4 (a).

It was observed that the *Nu* and *f* obtained from the present study exhibit good correlation with the established correlations. This agreement validates the accuracy and reliability of the numerical model used in this research. Furthermore, the Colburn j-factor was plotted against Reynolds number, as shown in Fig. 4(b). Based on the comparison between the results from the present study and the established correlations, it can be concluded that the numerical model employed in this study is reliable and capable of accurately simulating the HT and PD characteristics of the system under investigation.

4. Results and discussion

The current study focused on analyzing the impact of the magnetic field on the HT rate and fluid flow behavior of a hybrid nanofluid consisting of $Fe_3O_4 - TiO_2$. The computations were conducted using a finite volume method, and the obtained results were analyzed in terms of the *Nu*, *f*, Colburn j-factor and TEF.

Properties such as Nusselt number and friction factor have been presented in the results section as an average over top and bottom boundaries of the channel for the nanofluid employed in the present study. To calculate the average value of a property φ' at the top and bottom boundaries of the rectangular channel line averages were taken at each boundary using the following equation:

$$\varphi' = \frac{1}{l} * \int_0^l \varphi'_x dx \tag{21}$$

where l is the length of the channel and φ'_x is the local value of φ' at a distance x from the inlet.

4.1. Nusselt number analysis

The augmentation in the Nusselt number (*Nu*) resulting from the application of a magnetic field can be quantified through the ratio of *Nu* with the magnetic field (Nu_m) to *Nu* without the magnetic field (Nu_o), as summarized in Fig. 5. The observation that the ratio Nu_m/Nu_o is consistently greater than one for all cases indicates an increase in *Nu* in the presence of the magnetic field. This enhancement effect becomes more pronounced with higher magnetic field intensities, as seen in the increasing trend of Nu_m/Nu_o with the rise in magnetic field intensity.

Furthermore, the Nusselt number (*Nu*) shows a continuous increase with increasing Reynolds number (Re) as presented in Table 3. This consistent rise in *Nu* with increasing Re suggests that convective heat transfer improves as the fluid flow transitions from laminar to turbulent regimes. However, the impact of the magnetic field on *Nu* varies with the configuration of magnets. Among the different configurations studied, the curve corresponding to the magnet positioned at 7.5 mm shows lower enhancement compared to the curve for 15 mm, which in turn is lower than the curve for 25 mm. Similarly, the curve for the case with two magnets positioned at 25 mm and 32.5 mm is below the curve for the case with all four magnets in position. This trend is observed for all

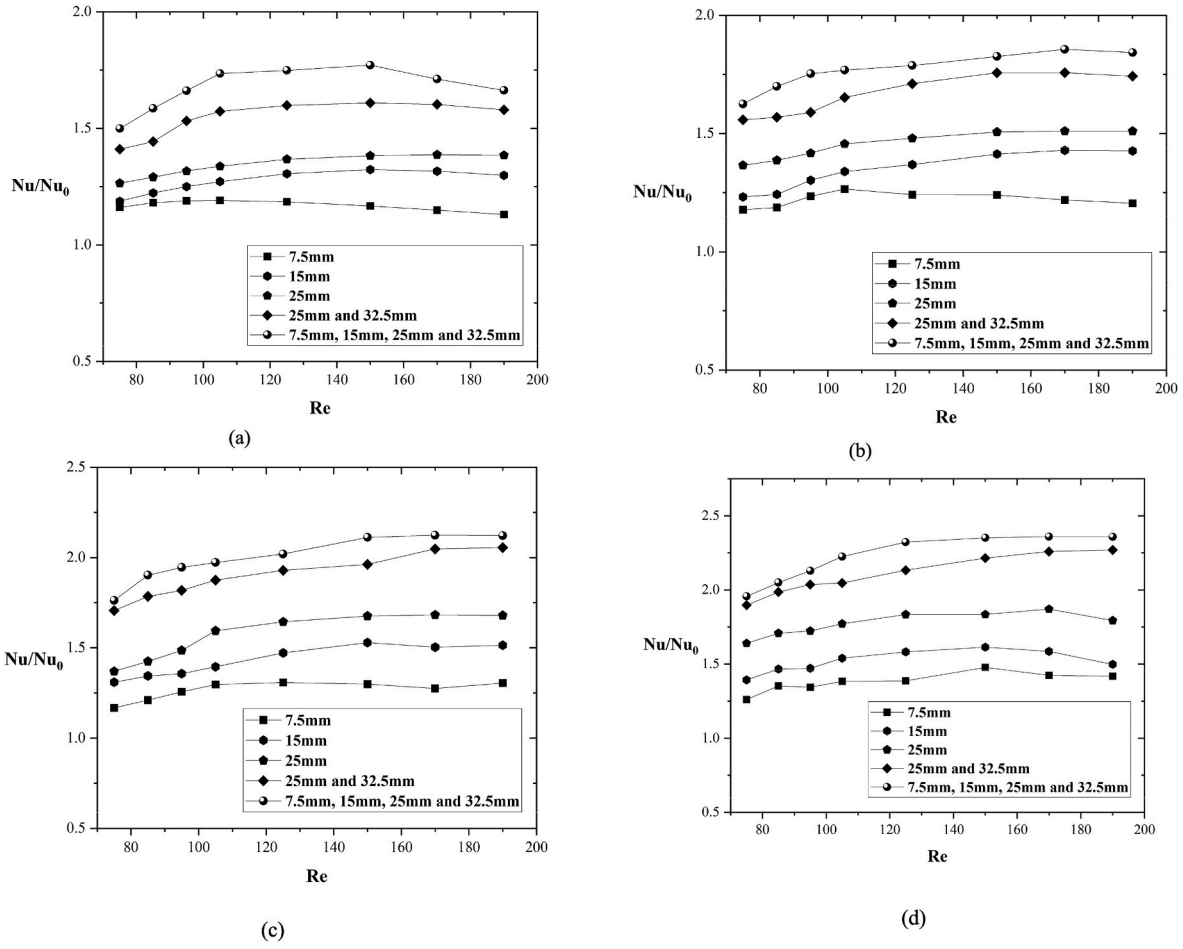

Fig. 5. *Nu*/Nu_o is the function of Reynolds number for various magnetic field intensities: (a) 1000G, (b) 1200G, (c) 1500G, and (d) 2000G.

Table 3
Nusselt number and friction factor enhancement for Re = 75.

Magnet(s) placement (mm)	Nusselt number					Friction factor				
	0G	1000G	1200G	1500G	2000G	0G	1000G	1200G	1500G	2000G
7.5	7.87	9.15	9.28	9.46	9.93	0.750	0.756	0.768	0.773	0.788
15	7.87	9.35	9.70	10.31	10.97	0.750	0.768	0.777	0.801	0.808
25	7.87	9.96	10.76	10.79	12.92	0.750	0.808	0.829	0.838	0.836
25 and 32.5	7.87	11.11	12.27	13.44	14.95	0.750	0.852	0.861	0.869	0.891
7.5, 15, 25 and 32.5	7.87	11.81	12.80	13.88	15.41	0.750	0.872	0.881	0.893	0.954

intensities of the magnetic field.

The relationship between the ratio of Nu_m/Nu_o and Reynolds number demonstrates a rising trend from Reynolds numbers of 75 until Reynolds number of 105, followed by a period of relative stability until a Reynolds number of 150, and afterwards a decline until a Reynolds number of 190. This observation suggests that the impact of the magnetic field on *Nu* is more prominent at lower and higher Reynolds numbers, while its influence diminishes at intermediate Reynolds numbers.

4.2. Colburn j-factor $\left[J = \frac{Nu}{Re \times Pr^{\frac{1}{3}}}\right]$ analysis

To provide physical reasoning for these quantitative results, we can consider the underlying mechanisms. The decrease in convective heat transfer efficiency (j-factor) with increasing Reynolds number in the laminar flow regime can be attributed to the increasing dominance of viscous forces over convective forces. As Re increases, the relative importance of inertial forces compared to viscous forces grows, leading to a decrease in convective heat transfer efficiency and a lower j-factor as shown in Fig. 6.

The increase in the j-factor with increasing magnetic field intensity can be explained by the influence of the magnetic field on the fluid flow. When a magnetic field is applied, it induces Lorentz forces that act on the conducting fluid. These Lorentz forces can suppress turbulence and enhance flow stability, resulting in improved convective heat transfer and increased j-factor.

The presented quantitative results highlight the significant impact of the magnetic field on the Nusselt number and suggest that the enhancement effect is more pronounced with higher magnetic field intensities. The consistent increase in *Nu* with increasing Re indicates improved heat transfer performance in the system. The underlying rationale for these observations can be attributed to the interaction between viscous and convective forces, as well as the influence of Reynolds number and the impact of Lorentz forces generated by the magnetic field on fluid flow. These factors collectively alter the efficiency of

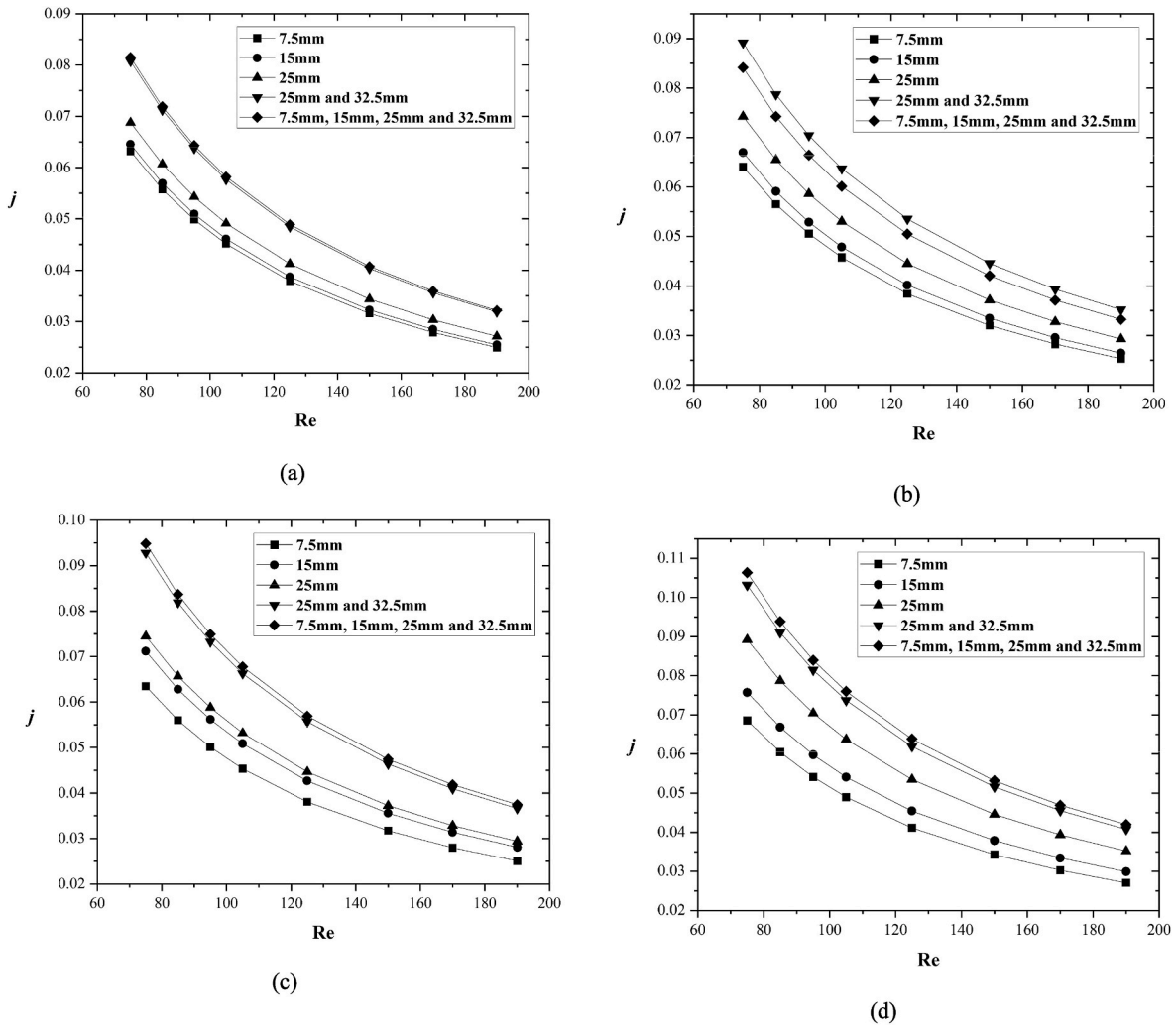

Fig. 6. Colburn j-factor is the function of Reynolds number for various magnetic field intensities: (a) 1000G, (b) 1200G, (c) 1500G, and (d) 2000G.

convective heat transfer.

4.3. Friction factor analysis

The trends observed in Fig. 7 for the friction factor (f) can be explained through physical reasoning based on the influence of the magnetic field and Reynolds number (Re) on fluid flow.

As Reynolds number increases, the decrease in friction factor can be attributed to the increasing dominance of viscous forces over inertial forces. In the laminar flow regime, the flow is mainly governed by viscous forces at lower Reynolds numbers, resulting in a higher friction factor. However, as Re increases, inertial forces become more significant, leading to a reduction in the relative importance of viscous forces, and thus, a decrease in the friction factor.

Similarly, the observed trends in friction factor with different magnet positions and magnetic field intensities can be explained based on the magnetic field's impact on fluid flow. The curve corresponding to the magnet positioned at 7.5 mm showing the lowest friction factor compared to the curves for 15 mm and 25 mm suggests that the magnetic field's influence on flow stability and turbulence suppression is more pronounced at closer distances to the magnets. The magnetic field's effect weakens as the distance increases, resulting in higher friction factors.

Moreover, the curve for the case with two magnets at 25 mm and 32.5 mm being below the curve for all four magnets in position indicates that the magnetic field's distribution plays a role. With all four magnets in place, the magnetic field has a more extensive and uniform effect, leading to increased flow stability and lower friction factors compared to the case with only two magnets.

The increased friction factor with increasing magnetic field intensity can be understood in terms of the interaction between the magnetic field and the conducting fluid. As the magnetic field intensity rises, the Lorentz forces induced in the fluid become stronger. These forces can influence the fluid flow, leading to a more structured and constrained flow, resulting in higher friction factors.

4.4. Thermal enhancement factor analysis

The observed behavior of the thermal enhancement factor (TEF) provides valuable insights into the system's heat transfer (HT) characteristics under the influence of magnetic field intensity. The results depicted in Fig. 8(a) show that the TEF initially increases with Reynolds' number up to 120. This behavior can be attributed to the combined effect of fluid flow behavior and heat transfer enhancement facilitated by the magnetic field.

The increase in TEF up to Reynolds number of 120 is likely due to the magnetic field's impact on fluid flow stability and suppression of turbulence, which leads to improved convective heat transfer. The magnetic field-induced Lorentz forces enhance fluid mixing, thus aiding in better heat transfer throughout the system.

However, after reaching a peak at a Reynolds number of 120, the TEF decreases. This decline can be attributed to the increased influence of

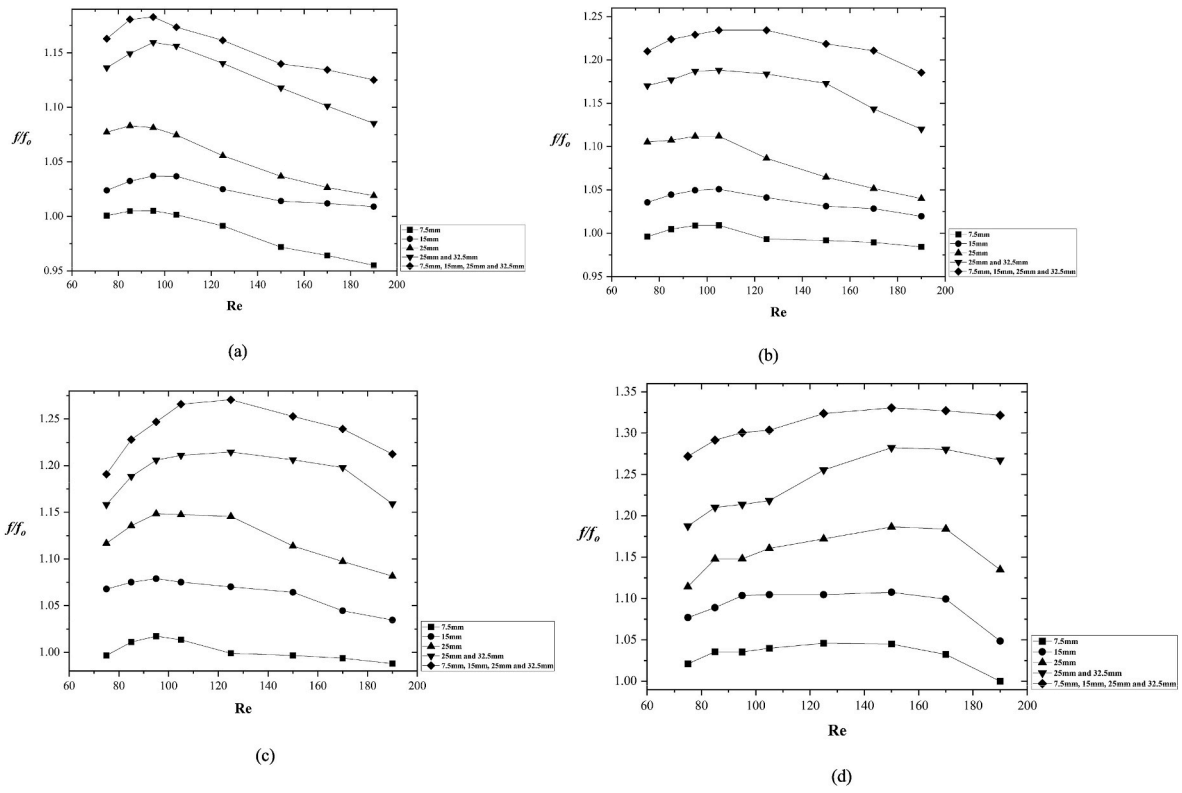

Fig. 7. Friction factor is the function of Reynolds number for various magnetic field intensities: (a) 1000G, (b) 1200G, (c) 1500G, and (d) 2000G.

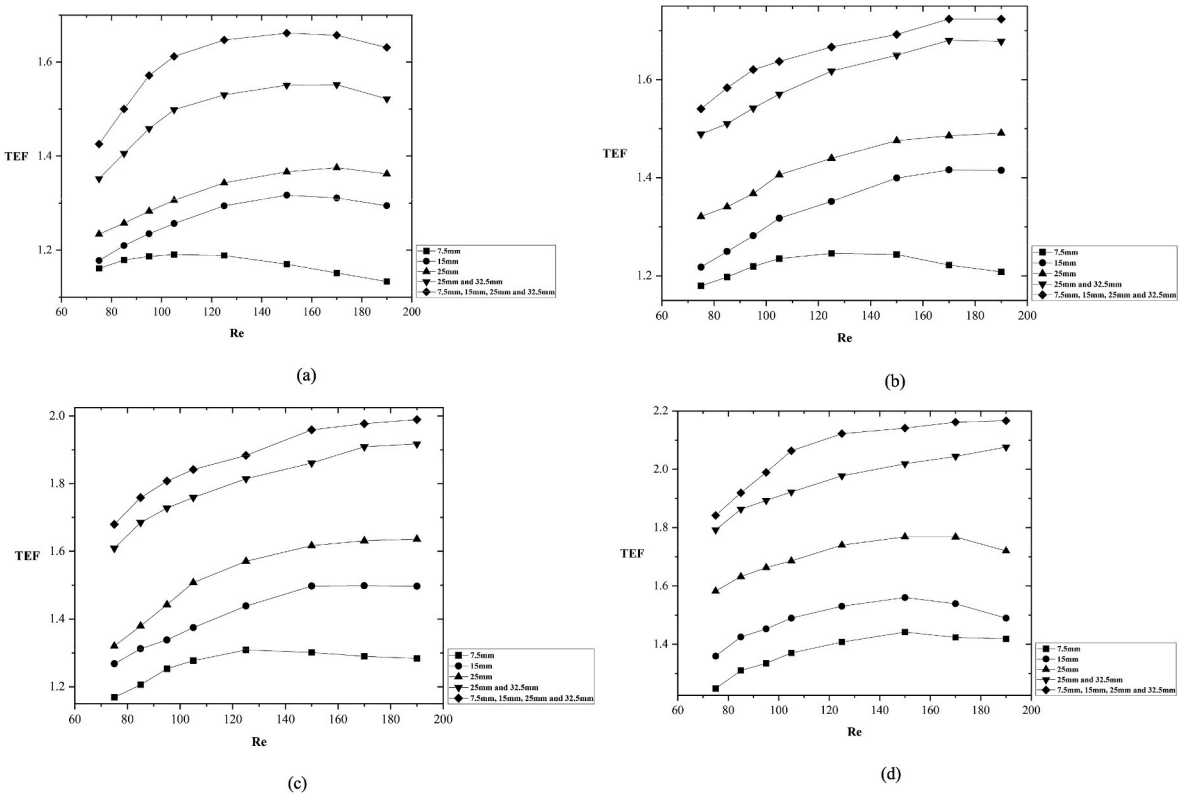

Fig. 8. TEF is the function of Reynolds number for various magnetic field intensities: (a) 1000G, (b) 1200G, (c) 1500G, and (d) 2000G.

the friction factor, which counteracts the heat transfer enhancement effects. The rise in friction factor is a consequence of the generation of vortices and increased turbulence caused by the magnetic field. These phenomena lead to higher energy losses and reduced heat transfer efficiency, resulting in a decrease in the TEF.

Nevertheless, when the magnetic field strength is increased, the

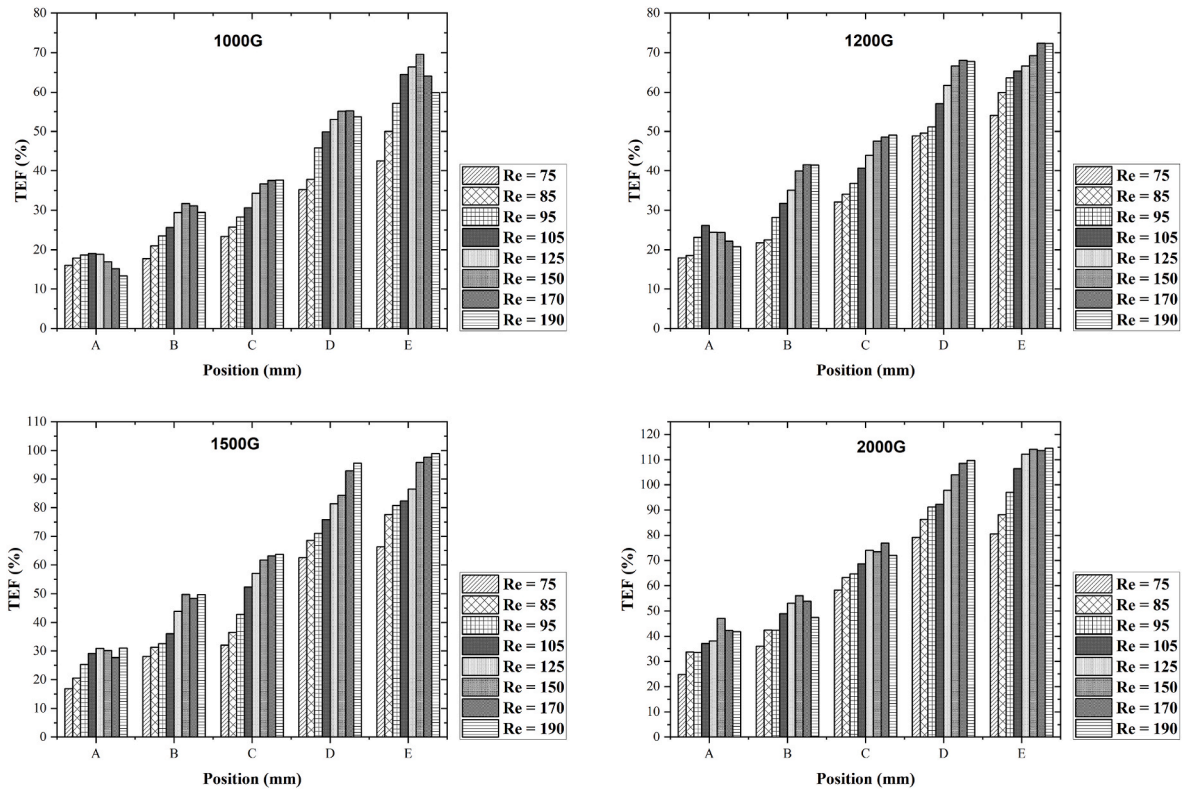

Fig. 9. Percentage enhancement in TEF with varying magnetic positions for (a) 1000G, (b) 1200 G, (c) 1500 G, (d) 2000 G intensity of magnetic field.

decline in TEF after a Reynolds number of 120 becomes less significant due to the intensified heat transfer enhancement effects brought about by the stronger magnetic field. The stronger magnetic field promotes even better fluid mixing, enhancing convective heat transfer and mitigating the negative impact of increased turbulence.

The TEF curve follows a similar trend in the cases of single magnets placed at different positions (Fig. 8(b), c, 8d). The decline in TEF after the Reynolds number of 120 is observed, but as the magnetic field strength increases, the curve tends to rise and approach parallelism with the x-axis at higher Reynolds numbers. Fig. 9 (a) to (d) illustrates the percentage enhancement in the thermal efficiency factor (TEF) as a function of varied magnet placements and varying strengths of the magnetic field.

The consistent emergence of TEF values exceeding 1 indicates an economically viable outcome, as the enhanced heat transfer more than compensates for the additional energy input. Furthermore, this underscores the potential for achieving improved heat exchange efficiency without compromising the overall energy balance. Our analysis using the TEF metric offers a positive outlook for our proposed approach's practicality and economic feasibility.

5. Conclusion

In conclusion, the HT enhancement was significantly affected by both the intensity and position of the magnetic field. The increase in magnetic field intensities and the judicious placement of magnets significantly impacted the investigated parameters. The study conducted on the effects of a magnetic field on a hybrid nanofluid consisting of Fe_3O_4–TiO_2 has yielded further significant observations.

1. A significant enhancement of up to 230% in the Nusselt number has been successfully attained under the influence of a magnetic field with a strength of 2000 G, at a Reynolds number of 190. This improvement was observed when all four magnets, placed at 7.5 mm, 15 mm, 25 mm, and 32.5 mm, were simultaneously activated.
2. A friction factor rise of up to 133% has been seen at a Reynolds number of 150 for a magnetic field strength of 2000 G when all four magnets placed at 7.5 mm, 15 mm, 25 mm, and 32.5 mm were activated, similar to the behavior exhibited by the Nusselt number.
3. A significant enhancement in TEF was also seen. The highest thermal enhancement factor (TEF) was seen at a Reynolds number of 190 when all four magnets placed at 7.5 mm, 15 mm, 25 mm, and 32.5 mm were activated with a magnetic field strength of 2000 G. In this particular instance, the TEF is calculated to be 2.18.
4. A minimum thermal enhancement factor (TEF) of 1.13 was observed at a Reynolds number of 190 for a magnetic strength of 1000 G when utilizing a single magnet placed at a location of 7.5 mm from the inlet.

These findings highlight the significant influence of magnetic fields on the HT characteristics of the Fe_3O_4–TiO_2 hybrid nanofluid. They emphasize the importance of magnetic field intensity, position, and fluid flow rate in optimizing heat transfer performance. The numerical results demonstrate the maximum enhancements in the *Nu*, *f*, Colburn *j*-factor and TEF, providing quantitative insights into the effectiveness of the magnetic field in enhancing HT in the system.

Declaration of competing interest

The authors declared that they have no conflict of interests.

Data availability

Data will be made available on request.

Acknowledgement

This work was supported by the Deanship of Scientific Research, the Vice Presidency for Graduate Studies and Scientific Research, King Faisal University, SaudiArabia (Grant No. 4347).

The authors also acknowledged the financial support received for the research project entitled "Performance Improvement of Solar Thermal Systems using Magnetic Nanofluids" funded by the Department of Science & Technology (DST), Govt. of India under India-South Africa Joint Science and Technology Research Collaboration vide Sanction no.: DST/INT/South Africa/P-08/2021 dtd. 16 Sept. 2021.

References

[1] L. Li, S. Feng, Y. Bai, X. Yang, M. Liu, M. Hao, S. Wang, Y. Wu, F. Sun, Z. Liu, et al., Enhancing hydrovoltaic power generation through heat conduction effects, Nat. Commun. 13 (1) (2022) 1043.
[2] J.B. Marcinichen, J.A. Olivier, N. Lamaison, J.R. Thome, Advances in electronics cooling, Heat Tran. Eng. 34 (5–6) (2013) 434–446.
[3] W. Jixiang, L. Yunze, L. Xiangdong, S. Chaoqun, H. Zhang, K. Xiong, Recent active thermal management technologies for the development of energy-optimized aerospace vehi- cles in China, Chin. J. Aeronaut. 34 (2) (2021) 1–27.
[4] Bergles, The implications and challenges of enhanced heat transfer for the chemical process industries, Chem. Eng. Res. Des. 79 (4) (2001) 437–444.
[5] S. Bhattacharyya, H. Chattopadhyay, A. Guin, A.C. Benim, Investigation of inclined turbulators for heat transfer enhancement in a solar air heater, Heat Tran. Eng. 40 (2019) 1451–1460, https://doi.org/10.1080/01457632.2018.1474593.
[6] B. Souayeh, S. Bhattacharyya, N. Hdhiri, F. Hammami, Numerical investigation on heat transfer augmentation in a triangular solar air heater tube fitted with angularcut varied-length twisted tape, Eur. Phys. J. A 136 (2021).
[7] Y. Hong, J. Du, S. Wang, S.M. Huang, W.B. Ye, Heat transfer and fluid flow behaviors in a tube with modified wire coils, Int. J. Heat Mass Tran. 124 (2018) 1347–1360, https://doi.org/10.1016/j.ijheatmasstransfer.2018.04.017.
[8] T. Wen, H. Zhan, D. Zhang, Flow boiling heat transfer in mini channel with serrated fins: experimental investigation and development of new correlation, Int. J. Heat Mass Tran. 128 (2019) 1081–1094, https://doi.org/10.1016/j.ijheatmasstransfer.2018.09.071.
[9] S. Xie, Z. Liang, L. Zhang, Y. Wang, A numerical study on heat transfer enhancement and flow structure in enhanced tube with cross ellipsoidal dimples, Int. J. Heat Mass Tran. 125 (2018) 434–444, https://doi.org/10.1016/j.ijheatmasstransfer.2018.04.106.
[10] S. Skullong, C. Thianpong, P. Promvonge, Effects of rib size and arrangement on forced convective heat transfer in a solar air heater channel, Heat Mass. Transf. Und. Stoffuebertragung 51 (2015) 1475–1485, https://doi.org/10.1007/s00231-015-1515-5.
[11] H.E. Fawaz, M.T.S. Badawy, M.F. Abd Rabbo, A. Elfeky, Numerical investigation of fully developed periodic turbulent flow in a square channel fitted with 45◦ in-line V-baffle turbulators pointing upstream, Alex. Eng. J. 57 (2018) 633–642, https://doi.org/10.1016/j.aej.2017.02.020.
[12] R. Rezazadeh, N. Pourmahmoud, S. Asaadi, Numerical investigation and performance analyses of rectangular mini channel with different types of ribs and their arrangements, Int. J. Therm. Sci. 132 (2018) 76–85, https://doi.org/10.1016/j.ijthermalsci.2018.05.048.
[13] Z. Feng, Y. Lan, Z. Hu, S. Zheng, Y. Zhang, Z. Huang, J. Zhang, Effects of longitudinal vortex generator pairs in transverse microchambers on thermal–hydraulic performances and entropy generation in an interrupted microchannel heat sink, J. Therm. Anal. Calorim. 147 (15) (2022) 8551–8567.
[14] E. Hosseinirad, F. Hormozi, Heat transfer improvement in a wavy vortex generator miniature channel using nanofluids, Heat Tran. Eng. 42 (2021) 409–430, https://doi.org/10.1080/01457632.2019.1703080.
[15] S. Skullong, P. Promvonge, N. Jayranaiwachira, C. Thianpong, Experimental and numerical heat transfer investigation in a tubular heat exchanger with delta-wing tape inserts, Chem. Eng. Process. Process Intensif. 109 (2016) 164–177, https://doi.org/10.1016/j.cep.2016.09.005.
[16] G. Liang, M.D. Islam, N. Kharoua, R. Simmons, Numerical study of heat transfer and flow behavior in a circular tube fitted with varying arrays of winglet vortex generators, Int. J. Therm. Sci. 134 (2018) 54–65, https://doi.org/10.1016/j.ijthermalsci.2018.08.00.
[17] K.N. Sneha, U.S. Mahabaleshwar, S. Bhattacharyya, An effect of thermal radiation on inclined mhd flow in hybrid nanofluids over a stretching/shrinking sheet, J. Therm. Anal. Calorim. 148 (Sep 2022) 2961–2975.
[18] M.B. Patil, K.C. Shobha, S. Bhattacharyya, Z. Said, Soret and dufour effects in the flow of casson nanofluid in a vertical channel with thermal radiation: entropy analysis, J. Therm. Anal. Calorim. 148 (Feb 2023) 2857–2867.
[19] Y. Khetib, H.M. Abo-Dief, A.K. Alanazi, S.M. Sajadi, S. Bhattacharyya, M. Sharifpur, Optimization of heat transfer in shell-and-tube heat exchangers using moga algorithm: adding nanofluid and changing the tube arrangement, Chem. Eng. Commun. 210 (Oct 2021) 893–907.
[20] A.A. Minea, Hybrid nanofluids based on al2o3, tio 2 and sio 2: numerical evaluation of different approaches, Int. J. Heat Mass Tran. 104 (2017) 852–860.
[21] Dongxu Jin, Shenglin Quan, Jianguo Zuo, Shiming Xu, Numerical investigation of heat transfer enhancement in a solar air heater roughened by multiple V-shaped ribs, Renew. Energy 134 (2019) 78–88, https://doi.org/10.1016/j.renene.2018.11.016. ISSN 0960-1481.
[22] Pongjet Promvonge, Skullong Sompol, Heat transfer augmentation in solar receiver heat exchanger with hole-punched wings, Appl. Therm. Eng. 155 (2019) 59–69, https://doi.org/10.1016/j.applthermaleng.2019.03.132. ISSN 1359-4311.
[23] Hüseyin Zahit Demirağ, Mehmet Doğan, Atila Abir İğci, The experimental and numerical investigation of novel type conic vortex generator on heat transfer enhancement, Int. J. Therm. Sci. 191 (2023), 108383, https://doi.org/10.1016/j.ijthermalsci.2023.108383. ISSN 1290-0729.
[24] M. Saadatmand, A.M. Goharkhah, Nejad, Heat transfer enhancement in mini channel heat sinks utilizing corona wind: a numerical study, Int. J. Heat Mass Tran. 182 (2022), 121970, https://doi.org/10.1016/j.ijheatmasstransfer.2021.121970.
[25] M. Gao, L.-S. Zhang, D.a. Zhang, L.-X. Zhang, Experimental study on the enhancement of free convection heat transfer under the action of an electric field, Exp. Therm. Fluid Sci. 104 (2019) 9–14.
[26] M. Bezaatpour, M. Goharkhah, Convective heat transfer enhancement in a double pipe mini heat exchanger by magnetic field induced swirling flow, Appl. Therm. Eng. 167 (Feb 2020), 114801.
[27] M. Bezaatpour, H. Rostamzadeh, Heat transfer enhancement of a fin-and-tube compact heat exchanger by employing magnetite ferrofluid flow and an external magnetic field, Appl. Therm. Eng. 164 (Jan 2020), 114462.
[28] Z. Lei, C. Haberstroh, S. Odenbach, K. Eckert, Heat transfer enhancement in magnetic cooling by means of magnetohydrodynamic convection, Int. J. Refrig. 62 (Feb 2016) 166–176.
[29] S. Bhattacharyya, A.K. Sharma, D.K. Vishwakarma, K. Saini, A.R. Paul, Z. Huan, Thermo-hydraulic performance of magnetic baffles for cooling using magnetic nanofluid in a mini channel, Sustain. Energy Technol. Assessments 57 (Jun 2023), 103194.
[30] S. Bhattacharyya, A.K. Sharma, D.K. Vishwakarma, A.R. Paul, Thermo-hydraulic characteristics of magnetic nanofluid in opposing and assisting mini-channel under the influ- ence of external magnetic field, Phys. Fluids 34 (Oct 2022), 103609.
[31] M. Sheikholeslami, B. Rezaeianjouybari, M. Darzi, A. Shafee, Z. Li, T.K. Nguyen, Application of nano-refrigerant for boiling heat transfer enhancement employing an exper- imental study, Int. J. Heat Mass Tran. 141 (Oct 2019) 974–980.
[32] M.A. Kumar, Y.D. Reddy, V.S. Rao, B.S. Goud, Thermal radiation impact on mhd heat transfer natural convective nano fluid flow over an impulsively started vertical plate, Case Stud. Therm. Eng. 24 (Apr 2021), 100826.
[33] A. Hajatzadeh Pordanjani, S. Aghakhani, A. Karimipour, M. Afrand, M. Goodarzi, Investigation of free convection heat transfer and entropy generation of nanofluid flow inside a cavity affected by magnetic field and thermal radiation, J. Therm. Anal. Calorim. 137 (Jan 2019) 997–1019.
[34] M. Ashjaee, M. Goharkhah, L.A. Khadem, R. Ahmadi, Effect of magnetic field on the forced convection heat transfer and pressure drop of a magnetic nanofluid in a miniature heat sink, Heat Mass. Transf. Und. Stoffuebertragung 51 (2015) 953–964, https://doi.org/10.1007/s00231-014-1467-1.
[35] M. Bezaatpour, M. Goharkhah, Three dimensional simulation of hydrodynamic and heat transfer behavior of magnetite nanofluid flow in circular and rectangular channel heat sinks filled with porous media, Powder Technol. 344 (2019) 68–78, https://doi.org/10.1016/J.POWTEC.2018.11.104.
[36] Pongjet Promvonge, et al., 3D simulation of laminar flow and heat transfer in V-baffled square channel, Int. Commun. Heat Mass Tran. 39 (1) (2012) 85–93.
[37] A.F. Mills, Basic Heat and Mass Transfer, Pearson College Division, 1999.
[38] J.E. Hesselgreaves, R. Law, D. Reay, Compact Heat Exchangers: Selection, Design and Operation, Butterworth-Heinemann, 2016.
[39] H. Bao, Y. Guo, S. Liu, C. Peng, Experimental study on natural circulation heat transfer of square channel in water-cooled blanket, IEEE Trans. Plasma Sci. 46 (6) (June 2018) 2291–2300, https://doi.org/10.1109/TPS.2018.2830643.